ELSEVIER

Journal of Structural Geology 27 (2005) 985–998

JOURNAL OF STRUCTURAL GEOLOGY

www.elsevier.com/locate/jsg

Structural signatures and $^{40}Ar/^{39}Ar$ geochronology of the Indosinian Xuefengshan tectonic belt, South China Block

Yuejun Wang[a,*], Yanhua Zhang[b], Weiming Fan[a], Touping Peng[a]

[a]*Key Laboratory of Isotope Geochronology and Geochemistry, Guangzhou Institute of Geochemistry, Chinese Academy of Sciences, Guangzhou 510640, People's Republic of China*

[b]*CSIRO Exploration and Mining, PO Box 1130, Bentley, WA 6102, Australia*

Received 5 August 2004; received in revised form 15 March 2005; accepted 1 April 2005

Available online 8 June 2005

Abstract

To advance our understanding of the kinematics of the Xuefengshan tectonic belt (XFSTB) and the Mesozoic tectonics of the South China Block (SCB), this paper presents new data and interpretations from our structural studies and thermochronological dating. The XFSTB is characterized by greenschist-facies metamorphism and development of S and S–L tectonic fabrics. An asymmetric positive flower structural pattern is composed of NW–WNW- and SE–ESE-dipping cleavages, faults and shear zones. Kinematic indicators indicate a dominant top-to-WNW-thrusting with a sinistral strike-slip component on the ESE-dipping shear zones and top-to-ESE-back-thrusting on the WNW-dipping shear zones. The quartz c-axis orientations of mylonitic rocks exhibit monoclinic point-maximum asymmetry, indicative of a sinistral shear sense under the ⟨a⟩ basal gliding condition. The timing of the major deformation event has been constrained to the middle Triassic to early Jurassic (244–195 Ma) on the basis of $^{40}Ar/^{39}Ar$ geochronology and other geological observations. The structural characteristics of the XFSTB are probably related to an Indosinian oblique convergent zone, in combination with tectonic wedging and associated back thrusting, all above a low-angle, SE-dipping basal detachment. Oblique northwestward and upward movement along the basal detachment was partitioned into the NW–WNW-directed thrusting, SE–ESE-directed back-thrusting and subsidiary strike-slip movement along the NE- and NNE-trending faults and shear zones. The XFSTB may represent part of a huge structural fan between the Yangtze and Cathaysian blocks, and can be interpreted as a product of the Indosinian intracontinental collision involving a weak zone.

Keywords: Tectonic fabrics; Positive flower structure; $^{40}Ar/^{39}Ar$ geochronology; Indosinian; Xuefengshan tectonic belt; South China Block

1. Introduction

Over the past 20 years, two distinct hypotheses have been proposed to account for the Mesozoic tectonic evolution of the South China Block (SCB) that is composed of the Yangtze and Cathaysian blocks (Fig. 1a; Li and McCulloch, 1996). One hypothesis suggests that the Mesozoic tectonic regime was dominantly compressive as a result of subduction of the Mesozoic Pacific plate or the oceanic crust within the SCB (Holloway, 1982; Hsü et al., 1990; Faure et al., 1996; Zhou and Li, 2000). This hypothesis advocated Mesozoic subduction/collision within the SCB evidenced by the 'Banxi ophiolite mélange' (Hsü et al., 1990) that is commonly called the Banxi Group in Chinese literature. However, more and more data show that the Banxi Group is a continuous Neoproterozoic sedimentary succession intruded by mafic–ultramafic plutons (HGBMR, 1988; Li, 1998; Wang et al., 2003). Furthermore, this hypothesis has also been challenged by paleomagnetic data, and the absence of an oceanic basin and Mesozoic island-arc magmatism within the SCB (Gupta, 1989; Rowley et al., 1989). The other hypothesis proposed that continental rifting was the dominant mechanism driving the tectonic evolution of the SCB since early Mesozoic or probably Paleozoic times (Rowley et al., 1989; Gilder et al., 1996; Wang et al., 2003a,b, 2005). Recent geochemical studies of the Mesozoic mafic rocks east of the XFSTB also strongly support the model of intracontinental lithospheric extension

* Corresponding author. Tel.: +86 20 85290527; fax: +86 20 85290708.
E-mail addresses: yjwang@gig.ac.cn (Y. Wang), wangyj6@21cn.com (Y. Wang).

0191-8141/$ - see front matter © 2005 Elsevier Ltd. All rights reserved.
doi:10.1016/j.jsg.2005.04.004

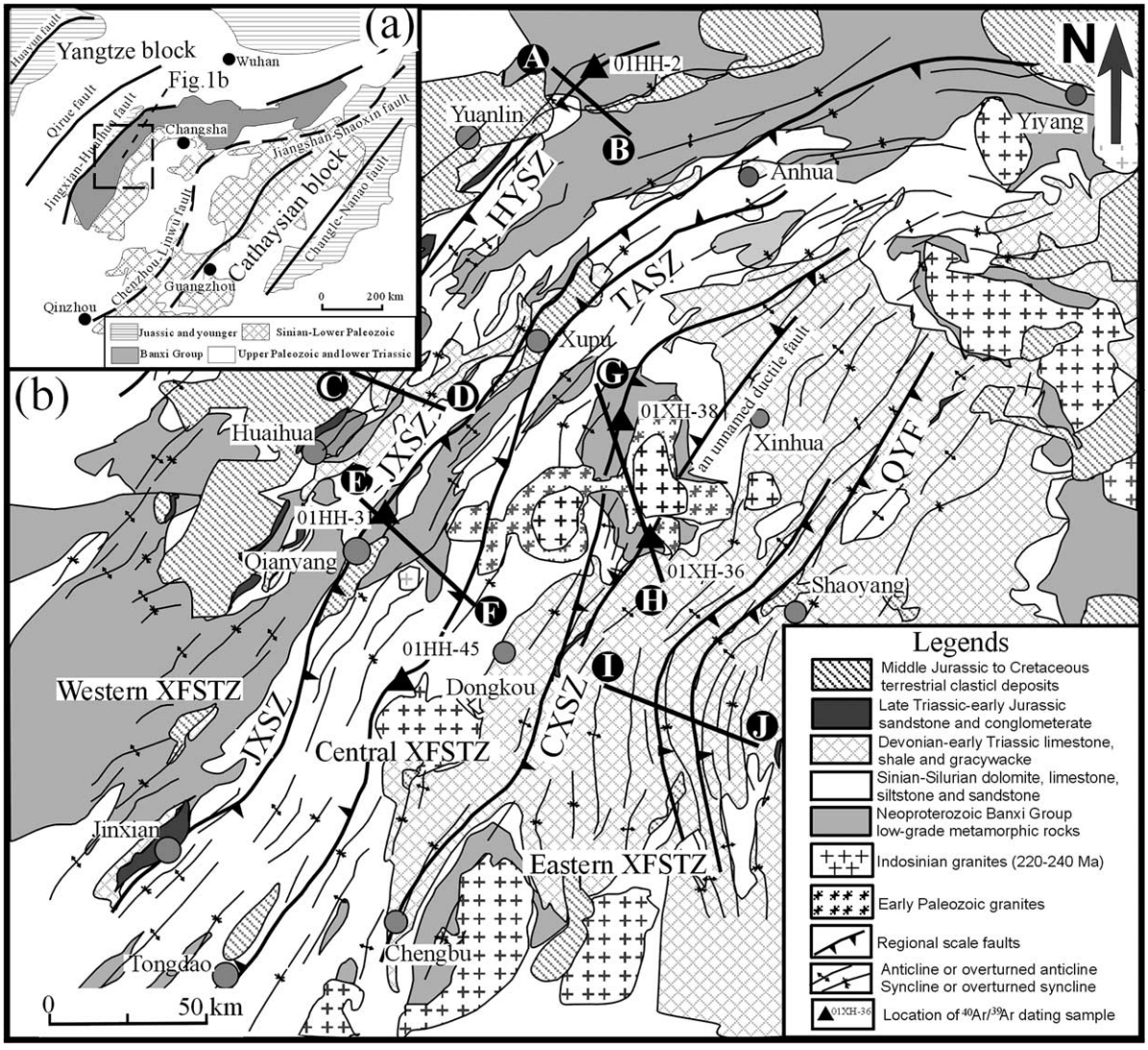

Fig. 1. (a) Tectonic sketch map of the South China Block (SCB) showing major faults and location of the study area (after Chen, 1999; Yan et al., 2003). (b) Geological map of the Xuefengshan tectonic belt (XFSTB), adapted from the 1:1,000,000 geological map of Hunan Province (HBGMR, 1988). The symbols of triangles refer to sampling locations for $^{40}Ar/^{39}Ar$ geochronology analyses. Locations of transects A–B, C–D, E–F, G–H, and I–J are also shown. HYSZ, JXSZ, TASZ, CXSZ and QYF represent the Huaihua–Yuanlin, Jinxina–Xupu, Tongdao–Anhua and Chengbu–Xinhua regional shear zones and the Qiyang arcuate brittle fault, respectively.

in response to an upwelling of asthenosphere since ca. 170 Ma (Wang et al., 2003a,b, 2005; Li et al., 2004). However, Chen (1999) reported that the Mesozoic structural pattern within the SCB is characterized by a NW-directed multilayer thrusting within the Yangtze block (Li, 1998; Yan et al., 2003) and SE-directed thrusting within the Cathaysian block (Charvet et al., 1994; Chen, 1999). Apparently, there is a lack of consensus about the Mesozoic tectonic evolution of the SCB.

To advance our understanding of the Mesozoic tectonic evolution of the SCB, it is vitally important to characterize the kinematic signatures recorded in the pre-Mesozoic rocks, and to constrain the timing of the major deformation event within the SCB. Although the structural styles and kinematics of several areas (e.g. the Wugongshan and Lushan metamorphic core complexes) have been described in previous literature (Faure et al., 1996; Chen, 1999; Lin et al., 2000; Yan et al., 2003), little attention has been paid to the structural significance of the XFSTB, and the timing of the major deformation event also remains unconstrained. In this paper, we present a synthesis of data from field mapping, structural studies and $^{40}Ar/^{39}Ar$ geochronological dating in the XFSTB. The XFSTB in western Hunan Province was selected for this study because it is a key tectonic mobile zone within the SCB, possibly representing the surface exposed boundary between the Yangtze and Cathaysian blocks (Fig. 1a). It is also an important tectonic zone containing major ductile high-strain zones, thrust-fold structures and extensive exposure of pre-Mesozoic strata within the SCB.

2. General geology

The XFSTB (Fig. 1b) is a NE-trending tectonic zone, 80–120 km wide and more than 200 km long, which developed along the surface exposed boundary between the Yangtze and Cathaysian blocks (HBGMR, 1988; Jia, 1992, 1994). From west to east, it contains the Huaihua–Yuanlin (HYSZ), Jinxina–Xupu (JXSZ), Tongdao–Anhua (TASZ) and Chengbu–Xinhua (CXSZ) regional scale shear zones and the Qiyang arcuate brittle fault (QYF). These structures form part of a NE-trending fault system within the SCB (Fig. 1a). The HYSZ, JXSZ, TASZ, and CXSZ were previously considered to be early Paleozoic thrust faults that were reactivated during the Indosinian orogeny, while the QYF was believed to be the product of the Indosinian orogeny (HBGMR, 1988; Jia, 1992, 1994).

The XFSTB is composed mainly of greenschist-facies metamorphic rocks. The stratigraphy of the XFSTB comprises the Neoproterozoic Banxi Group, Paleozoic shallow marine deposits and Mesozoic terrestrial sequences (HBGMR, 1988). The Banxi Group and its equivalents are traditionally considered to be the folded basement of the Yangtze block, although Hsü et al. (1988, 1990) suggested that they represent a Mesozoic mélange. Recent data indicate that the Banxi Group is mainly a well-bedded greywacke–slate–schist succession deposited at 760–820 Ma (Wang and Li, 2003; Wang et al., 2003; Yin et al., 2003). The Sinian strata are dominated by tillites and limestones, and the lower Paleozoic sequences include Cambrian slaty shales, sandstones and limestones, Ordovician limestones and argillaceous siltstones, and Silurian shales and sandstones. The Neoproterozoic and lower Paleozoic strata unconformably underlie the upper Paleozoic rocks and are metamorphosed into greenschist facies. The temperature and pressure of the metamorphism are approximately 300–450 °C and 4–6 kbar (HBGMR, 1988), respectively. The upper Paleozoic assemblage, unconformably overlain by upper Triassic and lower Jurassic terrestrial clastics, comprises middle and upper Devonian sandstones and siltstones, Carboniferous and Permian limestones and lower Triassic carbonate-rich rocks. The upper Triassic–lower Jurassic strata were regionally deformed during the development of the XFSTB, and were then intruded by the early Mesozoic granitoids of 172–180 Ma (HBGMR, 1988; Wang et al., 2003a). The sequences from middle Jurassic upwards are characterized by red terrestrial clastics, which display insignificant deformation fabrics and rest unconformably on the older rocks. Intrusions in the studied area, mainly exposed to the east of the JXSZ, include strongly deformed early Paleozoic granitoids (~420–450 Ma), weakly deformed Indosinian peraluminous granites (~220–245 Ma) and a small volume of undeformed Mesozoic intrusions (~120–180 Ma).

3. Structural signatures

Structural overprinting relationships associated with at least three deformation events can be identified in the XFSTB. Earlier deformation (D_1) is represented by rootless and hook-like folds, and by gently to steeply N-, NNE-, S-, and SSW-dipping foliations. D_1 structures have been largely transposed by subsequent deformation events. D_2 is a transpressive event that produced the dominant structural elements (e.g. folds, regional scale shear zones, foliations, and lineations) within the XFSTB. D_3 and subsequent deformation events are characterized by the development of brittle faults, although D_3 folds and small-scale ductile shear zones that overprint D_2 structures have been locally observed. In this study, special attention has been paid to the characteristics of D_2 structures, such as folds at various scales, pervasive cleavages, mylonitic foliations, stretching lineations, kinematic indicators, and quartz c-axis fabrics.

3.1. Cleavage

The most prominent D_2 structure is a well-developed cleavage throughout the XFSTB (mylonitic foliation in the shear zones is described separately in Section 3.3). In slates, phyllites and schists, the cleavage is represented by continuous and penetrative slaty to phyllitic foliation, and is defined by the preferred alignment of abundant fine-grained muscovite and sericite, and less amounts of chlorite and elongated quartz grains, with minute pressure shadow beards and seams of opaque materials. In siltstone and thin-bedded sandstone, the cleavage is closely spaced and defined by seams of opaque materials, the preferred alignment of muscovite, chlorite and quartz grains, and poorly developed pressure shadow beards. In thicker sandstone and limestone, the fabric is expressed as discontinuous, flaggy and spaced cleavage dominantly defined by seams of opaque materials and pressure shadow beards. An intensive cleavage is commonly observed in the Banxi Group and lower Paleozoic rocks. Cleavage intensity decreases in the Devonian and lower Triassic rocks that typically contain a spaced cleavage or fracture cleavage. These cleavages are commonly axial planar to folds, and generally trend NE and NNE and dip moderately to steeply towards both the east and west.

Cleavage orientations measured along five transects in the XFSTB are plotted in Fig. 2. In the western XFSTB west of the JXSZ, cleavage decreases in intensity with increasing distance to the HFSZ and JXSZ. The cleavage along transects A–B and C–D trends 015–045° and dips 40–80° to the SE (see stereograms in Fig. 2a and b). In the central XFSTB between the JXSZ and CXSZ, the intensity of the cleavage rapidly increases, and the dip angles of the cleavage decrease towards the JXSZ, TASZ and CXSZ. As shown in the transects E–F and G–H, the dip direction of a penetrative to spaced cleavage changes from NW and WNW on the southeastern flank to SE and ESE on the

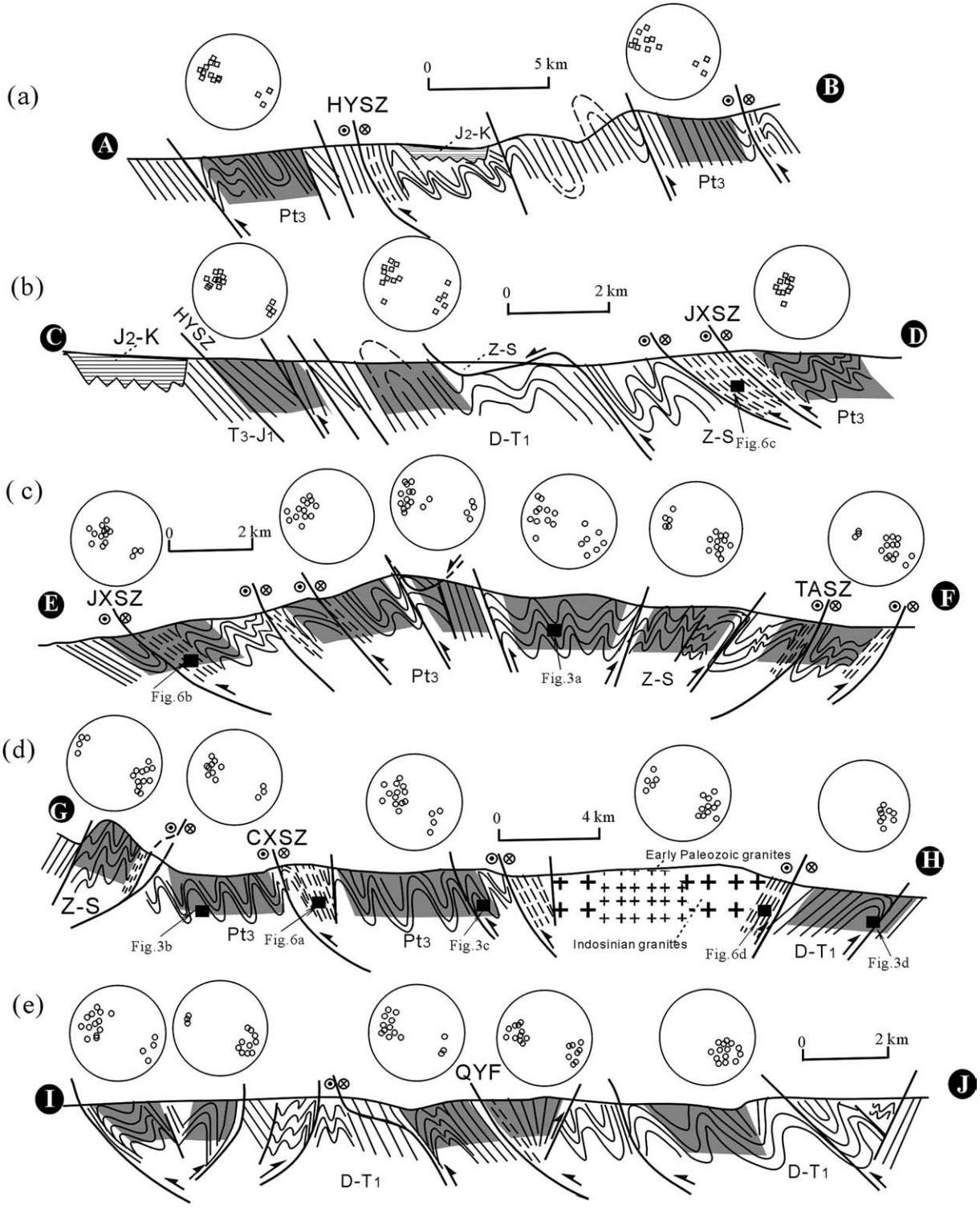

Fig. 2. Structural styles along the transects A–B (a), C–D (b), E–F (c), G–H (d), and I–J (e). See Fig. 1b for the locations of theses transects. Stereograms give the plots of cleavage orientations measured in the shaded areas along these transects in the XFSTB. Pt_3, Z–S and $D–T_1$, represent the Neoproterozoic Banxi Group, Sinian–Silurian and Devonian–lower Triassic marine strata, respectively, and $T_3–J_1$ and $J_2–K$ represent upper Triassic–lower Jurassic and middle Jurassic–Cretaceous terrestrial clastics, respectively. The locations of Figs. 3 and 6 are also shown.

northwestern flank of the central XFSTB (see Fig. 2c and d). Very steep cleavages are observed at the conjunctions between thrusting and back-thrusting faults in the central XFSTB. In the eastern XFSTB east of the CXSZ (Fig. 2e, transect I–J), the cleavage was heterogeneously developed, and a fan cleavage pattern defined by variations in dip direction was developed at the conjunction between thrusting and back-thrusting faults. The strike of the

cleavage along these transects varies in the range of 015–045°, and this is likely related to the extrusion of the XFSTB toward the NE and NNE, as predicated by an oblique convergence model (Braun and Beaumont, 1995).

3.2. Folds

Well-developed mesoscopic folds and associated faults in pre-Triassic sequences represent another group of major structural elements within the XFSTB. These folds have wavelengths ranging from tens of centimeters to a few meters, and most of them are overturned, recumbent, and tight to isoclinal folds accompanied by faults developed on their limbs (Fig. 3a–d). M-shape and asymmetrical Z-shape are the most common fold geometries. Folding in the upper Triassic and lower Jurassic rocks is less intensive. In the Banxi Group and Paleozoic rocks, folds usually have significantly thickened hinge zones and thinned/sheared limbs. Smaller-scale second order parasitic folds are observed within larger-scale folds and are usually preserved in the hinge zones of the latter, and both have subparallel axial planes (Fig. 3a–c). The macroscopic folds in the XFSTB (see Fig. 1b) have wavelengths of tens of kilometers. These folds commonly exhibit markedly asymmetric geometries, and most of them are overturned to either the NW–WNW or SE–ESE. Their axial planes generally trend NNE–NE, subparallel to the regional scale shear zones and faults. They are subvertical or dip moderately towards the SE–ESE or NW–WNW in the western and eastern parts of the XFSTB, respectively, but towards both the SE–ESE and NW–WNW in the central part of the XFSTB (see Fig. 2 for fold styles and their relationships with other structures). Such fold geometries suggest a roughly NW–SE shortening direction and dominant structural transport toward the NW.

3.3. Shear zones and faults

The Xuefengshan fault system is mainly composed of the NNE-trending regional scale shear zones and NE-trending faults. The NW-trending (310–345°) faults are locally developed. They usually dip steeply to the NE and cut across the NE-trending faults.

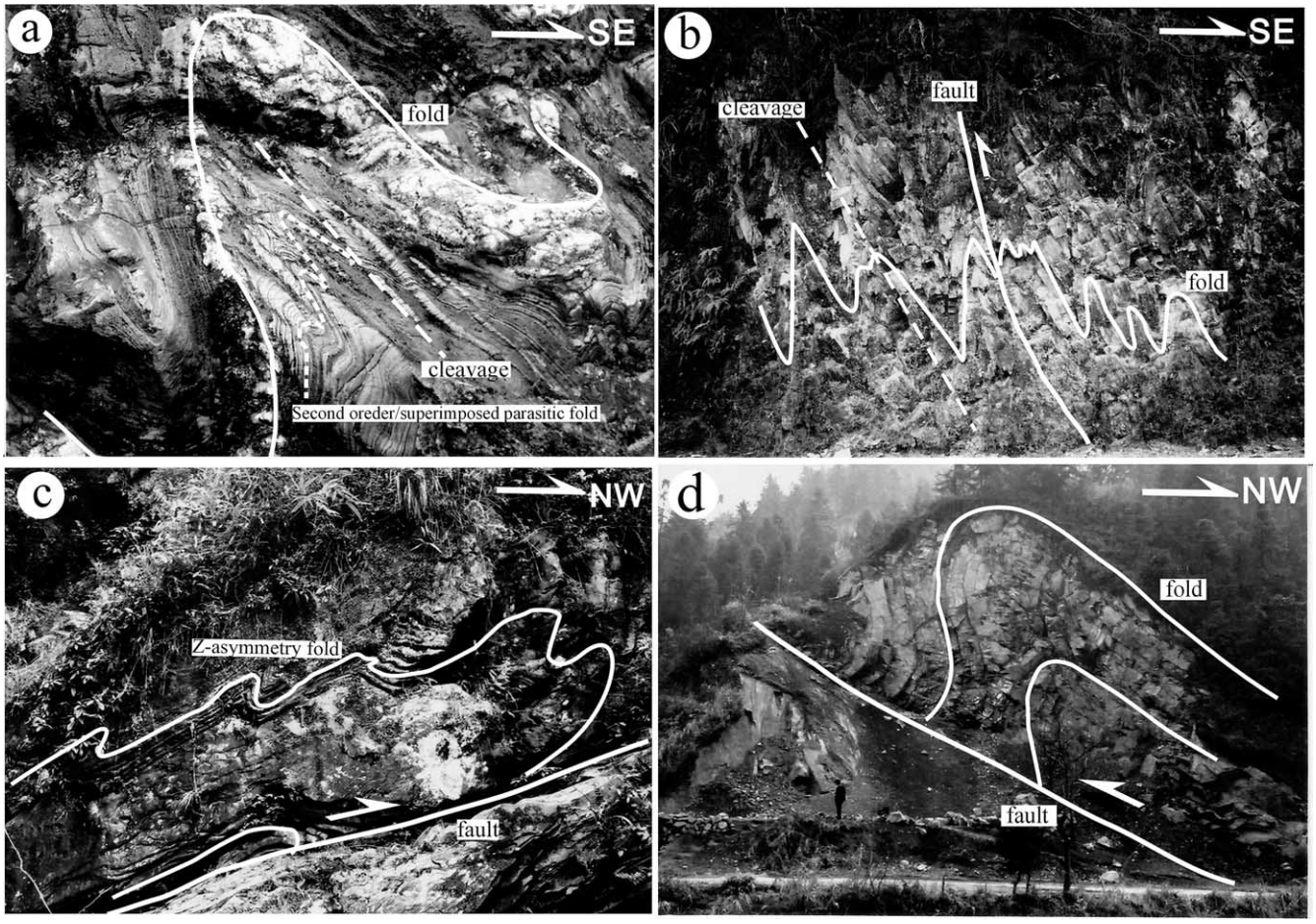

Fig. 3. Photographs showing structural relationships among cleavages, folds and thrust faults in the XFSTB. (a) Inclined tight folds with second order parasitic folds in the hinge zone (note that the axial planes of both are subparallel); (b) asymmetrical folds with axial planes subparallel to fault and cleavage; (c) a WNW-verging fold with an associated thrust fault; and (d) a NW-verging fold with an associated fault.

3.3.1. Regional scale shear zones

The NNE-trending regional scale shear zones include, from NW to SE, the HFSZ, JXSZ, TASZ and CXSZ (HBGMR, 1988; Jia, 1992). These shear zones all extend over 200 km, and their exposed widths vary from 50 to 2000 m. Strain distribution in these shear zones is highly heterogeneous. High strain zones with strong mylonitization (Fig. 4a and b) and marked tectonic fabrics often gradually transit into low strain zones with little or no mylonitization and fabric development. Deformed rocks within the shear zones commonly have similar metamorphic mineral assemblages composed of plagioclase, quartz, epidote, sericite, and muscovite ± biotite ± chlorite ± opaque minerals, and are mainly characterized by the development of S and S–L tectonic fabrics. The S-tectonites have mylonitic foliations (Fig. 4a and b) defined by the preferred alignment of muscovite, biotite, chlorite, flattened quartz grains, pressure shadow beards, and seams of opaque materials. The S–L tectonites contain additional stretching lineation that is marked by elongated, preferably oriented quartz and feldspar rods, and the streaks of aligned plagioclase and biotite.

Fabric orientations for the tectonites from the shear zones are summarized in Figs. 5 and 6. Mylonitic foliation dominantly dips in two opposite directions, but has a consistent NE–NNE trend. Within the SE- and ESE-dipping HYSZ, JXSZ and CXSZ, the foliations generally dip to the SE and ESE, and the stretching lineations on the foliations plunge shallowly to moderately toward the SE and SSE (mostly SSE; Figs. 5a–c and 6). The dip angles of the foliations within these shear zones increase from NW to SE across the XFSTB. In contrast, mylonitic rocks within the TASZ and an unnamed shear zone east of the CXSZ contain moderately to steeply WNW- and NW-dipping foliations and stretching lineations mostly plunging 25–60° to the NNW (335–355°). Some stretching lineations plunging 25–34° to the SW (210–240°) are also observed on the steeply SE- and ESE-dipping foliations (Fig. 5d and e). Structures that can be used as shear-sense indicators (Law, 1990; Hiroshi, 1994; Twiss and Moores, 1994) are observed locally. The most common shear-sense indicators include structural lenses (Fig. 4c), S–C fabrics, σ- and δ-type porphyroblasts (Fig. 4d), mica flakes, biotite-bearing shear bands, and fibrous quartz and asymmetric chlorite pressure shadows around rigid feldspar grains. These kinematic indicators all suggest the involvement of a sinistral shear component along these shear zones.

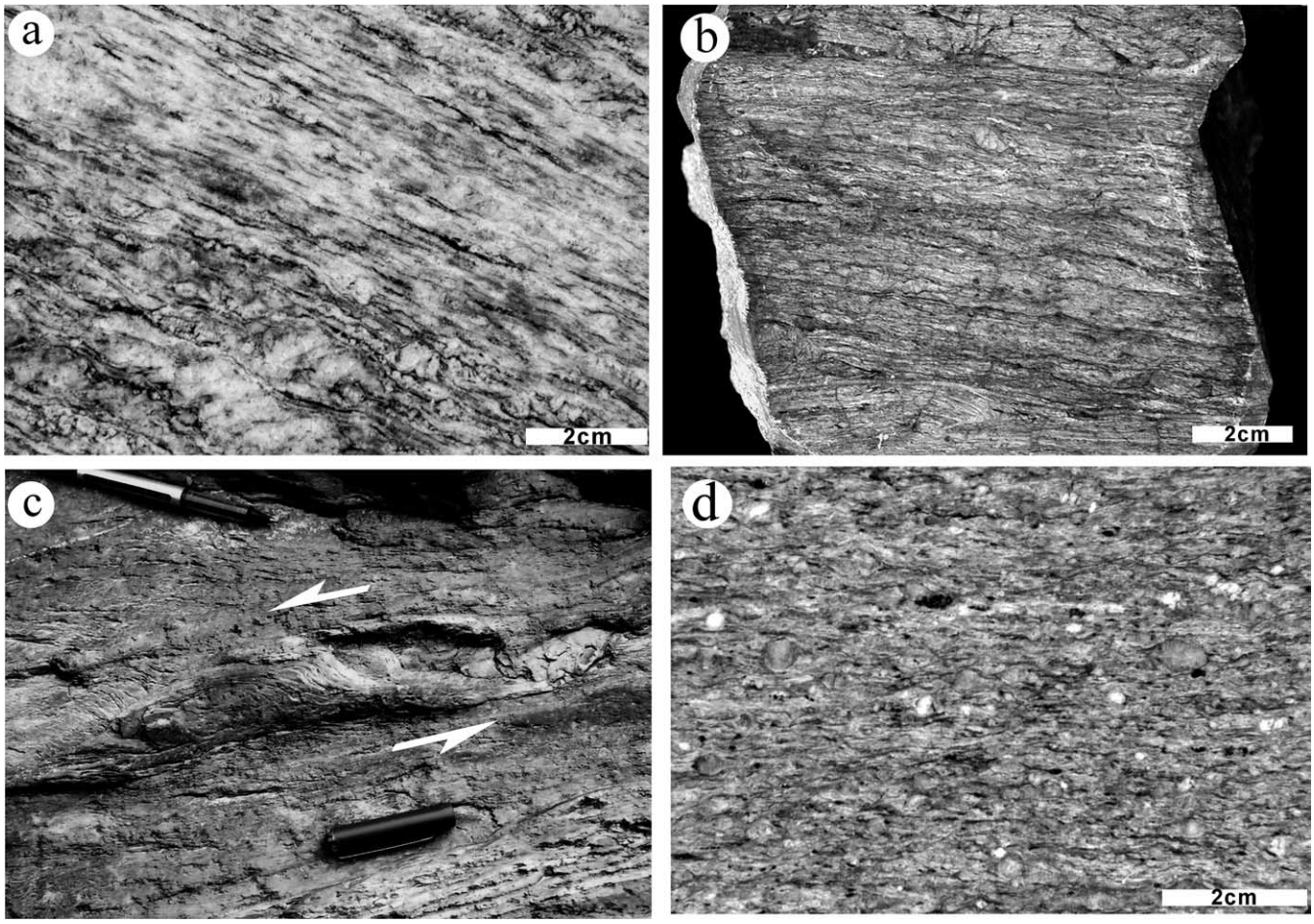

Fig. 4. Photographs showing strong mylonitization and mylonitic foliation (a) and (b), and sinistral shear sense ((c) structural lenses; (d) S–C fabrics).

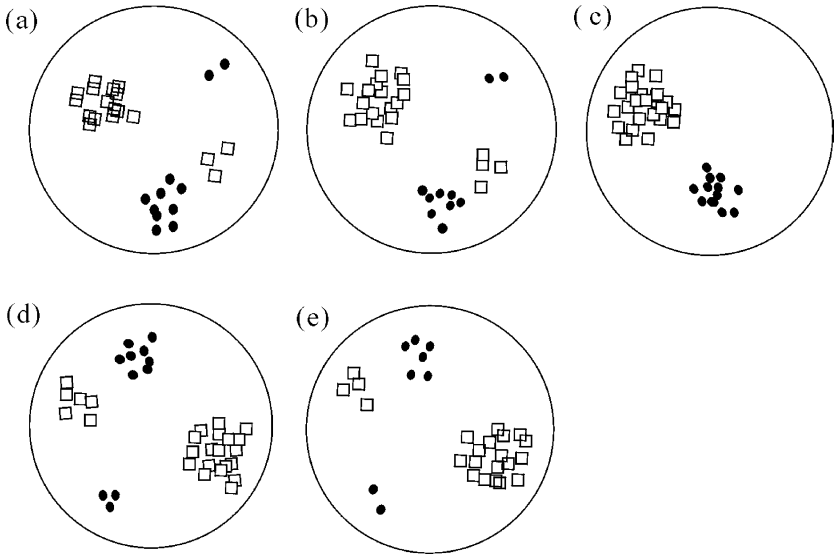

Fig. 5. Stereoplots (lower hemisphere, equal area) showing the dominant orientations of stretching lineations (dot), and poles to mylonitic foliations (square) in the NNE-trending shear zones within the XFSTB. (a) The Huaihua–Yuanlin shear zone (HYSZ); (b) the Jinxian–Xupu shear zone (JXSZ); (c) the Chengbu–Xinhua shear zone (CXSZ); (d) the Tongdao–Anhua shear zone (TASZ); and (e) an unnamed shear zone east of CXSZ.

3.3.2. NE-trending brittle faults

The NE-trending brittle faults (~30–60°) are generally ~10–20° to the NNE-trending shear zones (Fig. 6). They are commonly developed along the thinned limbs of folds, and are usually subparallel to or intersect with fold axial planes at low angles (Fig. 3b–d). They dip steeply to the SE in the western XFSTB (Fig. 2a and b), and to the SE or NW (predominantly to the SE) in the eastern XFSTB (Fig. 2e). In the central XFSTB, the faults dip steeply to both the SE and NW (Fig. 2c). These NE-trending faults probably merge with the moderately dipping HFSZ, JXSZ, TASZ and CXSZ at depth. The stratigraphic duplication of pre-Triassic sequences (older sequences rest over younger rocks) and the development of allochthonous slices are indicative of intensive thrusting. The geometries of the NE-trending faults probably reflect a positive flower structural pattern developed during transpressive deformation.

3.4. Quartz c-axis fabrics

The quartz c-axis preferred orientations of mylonitic rocks from the shear zones have been measured using a universal stage (Simpson and Schmid, 1983; Cobbold et al., 1987). Almost all the c-axis fabrics exhibit monoclinic point-maximum asymmetry with respect to the foliation and lineation orientation (Fig. 6), with major maxima almost normal to the relevant shear planes, which are consistent with the pattern commonly reported for non-coaxial deformation and can be used as a kinematic indicator (Bouchez et al., 1983; Law, 1990; Twiss and Moores, 1994), except for the sample 01HH-34.

The fabrics for the samples (01HH-10, -38, -45, -58 and 01XH-36, -42, -51) from the WNW-dipping shear zones (e.g. TASZ) are characterized by the densely populated maxima relatively near the Z-axis, which is probably indicative of the dominant activation of basal ⟨a⟩ gliding system (Tullis et al., 1973; Law, 1990). This gliding system generally activates at the conditions of lower temperatures (~300–400 °C) or higher strain rates (Tullis et al., 1973; Law, 1990; Twiss and Moores, 1994). Strong undulatory extinction of quartz grains and insignificant ductile deformation for feldspar in these samples also support the speculation that the deformation was under lower temperatures. The patterns of quartz c-axis fabrics for the samples (01HH-2, -12, -31, -52, and 01XH-19, -38) from the ESE-dipping shear zones (e.g., HYSZ, JXSZ and CXSZ) show maxima relatively near the Z-axis and also submaxima at positions between the Z- and Y-axes. This pattern probably indicates the activation of rhombohedral plane gliding system in addition to the operation of the basal ⟨a⟩ gliding system and thus the potential involvement of relatively higher temperatures (Twiss and Moores, 1994). Assuming that the geothermal gradient of the ESE-dipping shear zones is similar to that of the WNW-dipping shear zones, the different patterns of quartz c-axis fabric between them probably suggests that the rock samples from the latter were probably deformed at shallower levels under relatively lower temperatures, in comparison with those from the former. All the quartz c-axis fabric patterns suggest the sinistral sense of shearing along the NE-trending shear zones, consistent with the kinematic predictions of the meso- and microscopic structural evidences described above. The deformation temperatures of the shear zones are likely to be in the range of ~300–450 °C.

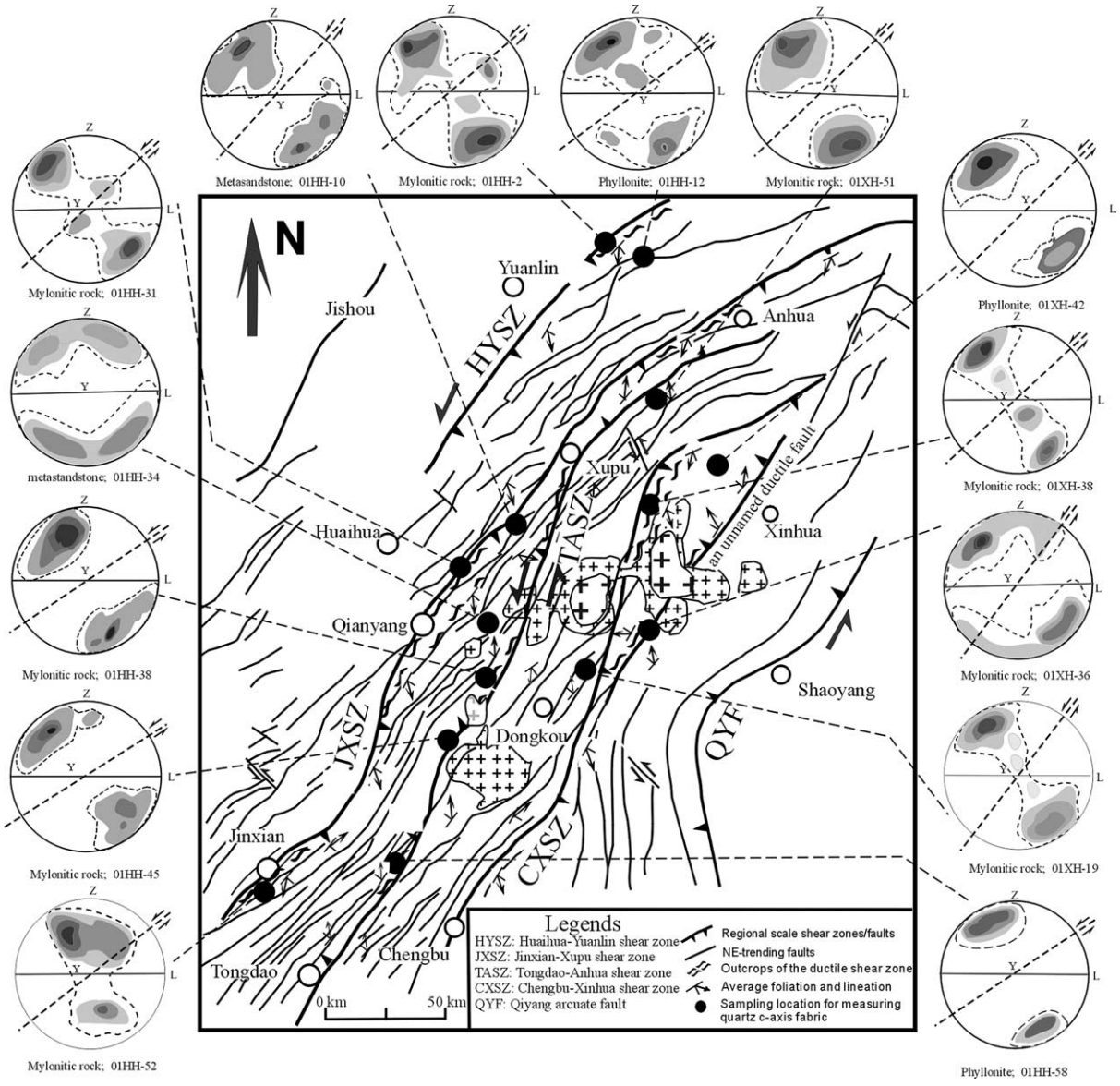

Fig. 6. Quartz c-axis orientation projections (lower hemisphere, equal area) for the mylonitic rocks, with about 120 data for each plot. L and Z represent the directions of the maximum elongation and shortening, respectively. Contour intervals are 1, 4, 7, and 10%. See text for more information.

4. Timing of deformation: mineral $^{40}Ar/^{39}Ar$ geochronology

The geochronological data of the deformed rocks within the SCB are presently sparse (Faure et al., 1996; Lin et al., 2000). In this study, to constrain the deformation age of the XFSTB, sericite, biotite, and muscovite separates from five samples (see Fig. 1b for their locations) were selected for dating by the $^{40}Ar/^{39}Ar$ radiometric stepwise heating method (Dalrymple and Lanphere, 1971; Maluski et al., 1993).

4.1. Analytical technique

The required mineral separates for $^{40}Ar/^{39}Ar$ dating were carefully handpicked under a binocular microscope. The mineral separates were individually wrapped in Al-foil packets, encapsulated in sealed Gd-foil, and irradiated at the central thimble position of the nuclear reactor (1000 kW) at the Chinese Academy of Atomic Energy Science for 2627 min with an instantaneous neutron flux of 6.63×10^{12} n/cm^2. After irradiation, the samples were progressively heated and degassed from 420 to 1450 °C. Purified argon was finally collected using a Zr–Al getter pump, and subsequently analyzed with a RGA-10 gas source mass-spectrometer operated in the static mode at the Institute of Geology and Geophysics, the Chinese Academy of Sciences. The analytical procedures are the same as reported by Sang et al. (1996). Total uncertainties in each apparent age have been calculated using the methods outlined by Dalrymple and Lanphere (1971). An internal standard Biotite GA1550 was used as a monitor to calibrate the

J value, the age of which is 97.9±0.7 Ma. These results are summarized in Table 1 and shown in Fig. 7.

4.2. Mineral $^{40}Ar/^{39}Ar$ dating results

A mylonite sample (01HH-2) containing fine-grained elongated quartz was taken from the HYSZ (Guanzhuang, Yuanlin). The sample yields relatively flat $^{40}Ar/^{39}Ar$ apparent age spectra during intermediate–high temperature heating steps, giving a plateau age of 194.7±0.3 Ma defined by ~78% released gas (Fig. 7a). Biotite separates from a mylonitic gneiss (01HH-31) in the JXSZ (Chanziping, Qianyang) yield variable apparent age during low temperature steps but well-defined plateau age with slightly variable $^{37}Ar/^{39}Ar$ ratios during intermediate–high temperature heating steps. A plateau age of 216.9±0.3 Ma is well defined by >89% ^{39}Ar released (Fig. 7b). The sericite separates from a mylonitic schist (01HH-45), representative of ductilely deformed rocks in the TASZ (Nuoxi, Dongkou), yield a plateau age of 207.2±0.2 Ma (>85% ^{39}Ar released, Fig. 7c). The muscovite separates of two fine-grained mylonitic samples from the CXSZ (Guliangqiao, Xinhua, 01XH-38) and the unnamed shear zone east of the CXSZ (Yanggu'ao, Longhui, 01XH-36), record the $^{40}Ar/^{39}Ar$ plateau ages of 215.3±0.8 and 213.5±0.2 Ma with over 85% ^{39}Ar release (Fig. 7d and e), respectively. All plateau ages are comparable with their isochron ages, and the inverse ordinate intercepts (289.3–306.6) are close to the $^{40}Ar/^{36}Ar$ ratio of the present-day atmosphere (295.5).

4.3. Timing of deformation

The timing of deformation in the XFSTB can be synthetically constrained by the deformation ages of

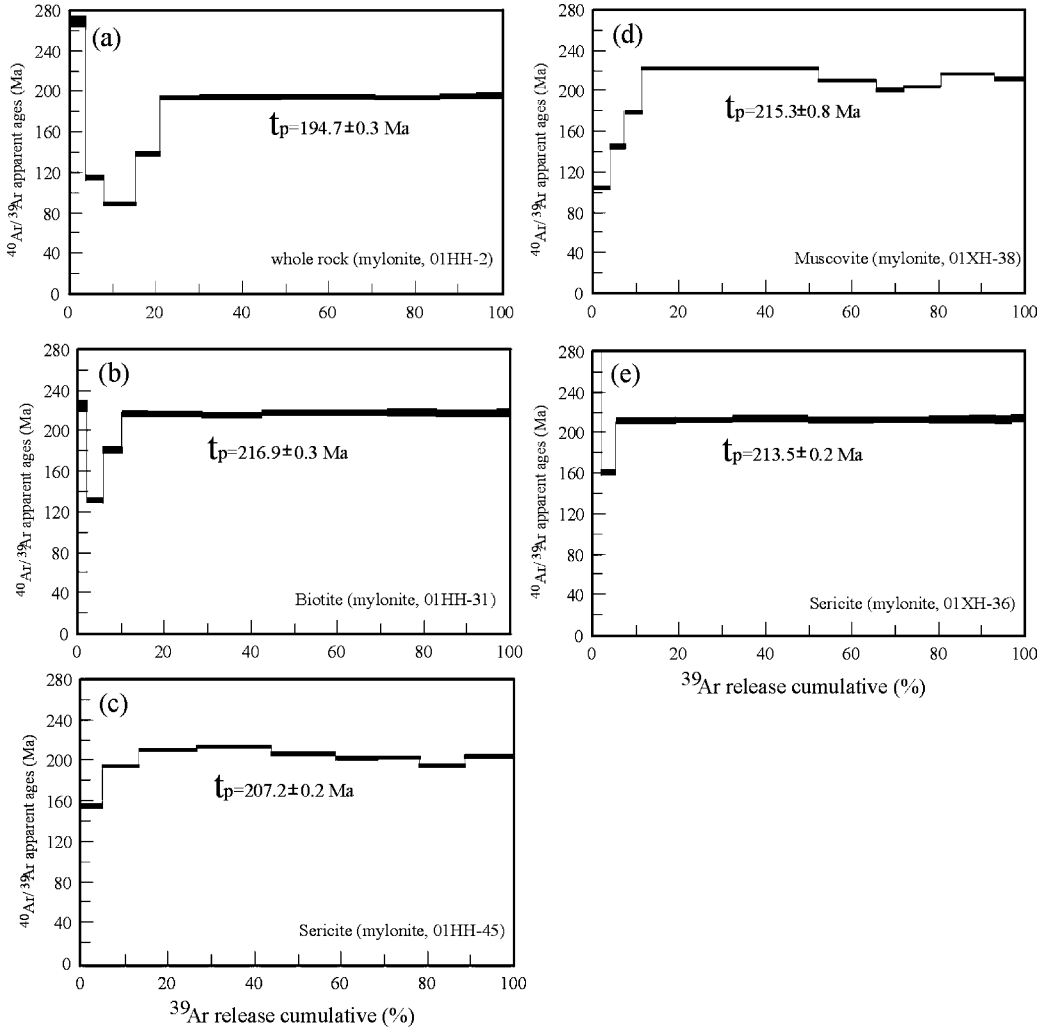

Fig. 7. The $^{40}Ar/^{39}Ar$ apparent age spectra of mineral separates from mylonitic rocks. (a) 01HH-2 at Guangzhuang (Yuanling), representative of the HYSZ; (b) 01HH-31 at Chanziping (Qianyang), representative of the JXSZ; (c) 01HH-45 at Nuoxi (Dongkou), representative of the TASZ; (d) 01XH-38 at Guliangqiao (Xinhua), representative of the ESE-dipping CXSZ; (e) 01XH-36 at Yanggu'ao (Longhui), representative for a small-scale NW-dipping back-thrusting shear zone. Coarse lines give the apparent ages (the length of bars reflects 1σ uncertainty). See Fig. 1b for the locations of the samples.

Table 1
$^{40}Ar/^{39}Ar$ isotopic analytical results for incremental heating experiments on mineral separates and whole rock from the Xuefengshan regional shear zones

Temperature (°C)	$(^{40}Ar/^{39}Ar)_m$	$(^{36}Ar/^{39}Ar)_m$	$(^{37}Ar/^{39}Ar)_m$	$(^{38}Ar/^{39}Ar)_m$	$^{39}Ar_k$ (10^{-12} mol)	$(^{40}Ar/^{39}Ar_k)$ ($\pm1\sigma$)	$^{39}Ar_k$ (%)	Apparent age ($t\pm1\sigma$ Ma)
Mylonite (01HH-2), weight = 0.1615 g, J = 0.01088, Plateau age: 194.7 ± 0.3 Ma								
420	25.336	0.0358	0.4197	0.0645	5.172	14.79 ± 0.020	3.03	269.25 ± 5.85
550	10.027	0.0136	0.2673	0.0444	8.512	6.014 ± 0.004	5.00	114.34 ± 1.43
650	9.011	0.0149	0.2230	0.0406	12.430	4.610 ± 0.003	7.30	88.31 ± 1.09
750	11.609	0.0015	0.3933	0.0646	9.509	7.312 ± 0.006	5.58	138.10 ± 1.84
850	12.992	0.0087	0.2600	0.0398	15.880	10.41 ± 0.005	9.33	193.57 ± 2.46
950	12.666	0.0074	0.1378	0.0218	31.310	10.46 ± 0.004	18.30	194.62 ± 2.40
1050	12.303	0.0060	0.1264	0.0203	38.270	10.50 ± 0.004	22.40	195.18 ± 2.38
1150	12.666	0.0076	0.1643	0.0299	24.350	10.41 ± 0.005	14.60	193.58 ± 2.40
1300	13.281	0.0093	0.2167	0.0332	14.840	10.51 ± 0.005	8.72	195.39 ± 2.47
1450	14.004	0.0117	0.2456	0.0437	9.904	10.55 ± 0.006	5.81	196.10 ± 2.57
Inverse isochron age: 193.1 ± 0.3 Ma, $^{40}Ar/^{36}Ar$ ratio = 306.6								
Biotite (01HH-31), weight = 0.1037 g, J = 0.01257, Plateau age: 216.9 ± 0.3 Ma								
420	18.406	0.0268	0.1613	0.0724	6.912	10.52 ± 0.021	2.21	224.13 ± 5.16
550	10.743	0.0161	0.0966	0.0394	14.350	5.998 ± 0.007	4.59	131.12 ± 1.79
660	13.306	0.0168	0.1434	0.0620	11.060	8.388 ± 0.011	3.54	180.82 ± 2.91
760	12.287	0.0073	0.1012	0.0437	18.860	10.12 ± 0.009	6.04	216.11 ± 3.14
840	11.204	0.0036	0.0753	0.0261	38.510	10.14 ± 0.007	12.30	216.53 ± 2.91
920	11.005	0.0031	0.0887	0.0345	43.840	10.07 ± 0.007	14.00	215.16 ± 2.89
1040	11.099	0.0030	0.0954	0.0362	45.930	10.20 ± 0.008	29.30	217.68 ± 2.94
1160	11.418	0.0040	0.1018	0.0395	34.330	10.23 ± 0.008	10.90	218.30 ± 3.01
1280	12.109	0.0066	0.1199	0.0499	21.755	10.17 ± 0.009	13.93	216.91 ± 3.16
1420	14.739	0.0156	0.1948	0.0807	8.910	10.16 ± 0.014	2.85	216.87 ± 3.91
Inverse isochron age: 216.7 ± 0.4 Ma, $^{40}Ar/^{36}Ar$ ratio = 291.9								
Sericite (01HH-45), weight = 0.1183 g, J = 0.00964, Plateau age: 207.2 ± 0.2 Ma								
360	16.960	0.0244	0.0121	0.0371	4.557	9.809 ± 0.104	4.52	157.17 ± 1.68
520	14.425	0.0072	0.0067	0.0233	8.875	12.35 ± 0.075	8.80	195.82 ± 1.59
680	14.384	0.0027	0.0048	0.0208	30.065	13.62 ± 0.033	13.64	214.88 ± 0.52
750	14.096	0.0026	0.0057	0.0220	14.890	13.07 ± 0.053	16.74	210.76 ± 0.87
810	13.807	0.0026	0.0067	0.0231	9.968	12.86 ± 0.076	14.76	206.63 ± 1.21
870	13.602	0.0027	0.0111	0.0287	9.655	12.90 ± 0.066	9.88	203.44 ± 1.21
980	13.613	0.0026	0.0093	0.0260	10.571	12.41 ± 0.053	9.57	204.03 ± 1.06
1030	13.107	0.0025	0.0081	0.0249	10.938	12.68 ± 0.060	10.48	196.69 ± 0.84
1340	13.645	0.0026	0.0091	0.0241	11.727	12.92 ± 0.064	11.62	204.44 ± 1.01
Inverse isochron age: 206.1 ± 0.2 Ma, $^{40}Ar/^{36}Ar$ ratio = 289.3								
Muscovite (01XH-38), weight = 0.1167 g, J = 0.00938, Plateau age: 215.3 ± 0.8 Ma								
360	7.631	0.0047	0.0080	0.0277	6.990	6.269 ± 0.085	4.51	103.37 ± 1.41
520	9.714	0.0030	0.0149	0.0619	5.068	8.910 ± 0.134	3.27	144.61 ± 2.20
680	11.585	0.0021	0.0107	0.0310	6.418	11.04 ± 0.100	4.14	177.58 ± 1.62
750	14.034	0.0004	0.0016	0.0155	63.537	13.93 ± 0.041	41.02	221.62 ± 0.66
810	13.318	0.0004	0.0037	0.0188	20.938	13.21 ± 0.041	13.52	210.69 ± 0.66
870	12.535	0.0002	0.0092	0.0315	9.357	12.49 ± 0.111	6.04	200.55 ± 1.78
980	12.747	0.0002	0.0085	0.0257	12.672	12.28 ± 0.047	8.18	203.35 ± 0.75
1030	13.810	0.0007	0.0032	0.0185	19.230	13.60 ± 0.031	12.41	216.68 ± 0.50
1340	2.3958	0.0017	0.0291	0.0163	10.690	13.26 ± 0.064	6.90	211.49 ± 1.03
Inverse isochron age: 204.7 ± 1.2 Ma, $^{40}Ar/^{36}Ar$ ratio = 296.5								
Muscovite (01XH-36), weight = 0.0914 g, J = 0.01725, Plateau age: 213.5 ± 0.2 Ma								
420	22.802	0.0171	0.0627	0.0653	6.10	17.77 ± 0.041	2.10	367.90 ± 14.53
540	11.579	0.0141	0.0650	0.0508	9.81	7.421 ± 0.011	3.38	162.62 ± 2.59
640	12.155	0.0077	0.0404	0.0367	17.86	9.866 ± 0.012	6.15	213.37 ± 3.43
720	11.958	0.0072	0.0493	0.0345	22.50	9.839 ± 0.011	7.75	212.82 ± 3.37
800	11.280	0.0048	0.0420	0.0218	38.04	9.847 ± 0.010	13.10	212.98 ± 3.17
880	11.302	0.0046	0.0348	0.0185	49.87	9.934 ± 0.010	17.10	214.76 ± 3.20
960	10.645	0.0026	0.0375	0.0202	43.15	9.855 ± 0.009	14.80	213.15 ± 3.03
1040	10.915	0.0036	0.0339	0.0207	38.51	9.853 ± 0.009	13.20	213.10 ± 3.09
1120	11.596	0.0058	0.0366	0.0262	27.60	9.867 ± 0.010	9.51	213.40 ± 3.26
1200	12.361	0.0083	0.0482	0.0341	16.70	9.912 ± 0.012	5.75	214.32 ± 3.50
1300	13.275	0.0116	0.0607	0.0374	11.97	9.859 ± 0.014	4.12	213.22 ± 3.77
1400	15.117	0.0176	0.0697	0.0420	7.89	9.932 ± 0.018	2.71	214.71 ± 4.48
Inverse isochron age: 213.1 ± 0.4 Ma, $^{40}Ar/^{36}Ar$ ratio = 297.4								

Noting: parameter $\lambda = 5.543\times10^{-10}$/a; $(^{40}Ar/^{39}Ar)_m$: measured values of $^{40}Ar/^{39}Ar$; $^{39}Ar_k$: measured values of $^{39}Ar_k$, which was produced by k decay.

mylonitic rocks, the crystallization ages of syntectonic granites and post-tectonic intrusions, and stratigraphic relationship in the study area. As noted above, the dated minerals aligned along the foliation in greenschist-facies metamorphic rocks were probably recrystallized during the D_2 deformation event. Quartz c-axis fabrics are dominated by basal ⟨a⟩ gliding patterns with the deformation temperatures of ~300–450 °C. The aforementioned $^{40}Ar/^{39}Ar$ plateau ages of 195–216 Ma, representing the timing of cooling through appropriate argon closure temperatures in muscovite and sericite (350–400 °C; Purdy and Jäger, 1976; Harrison et al., 1985) and in biotite (300–350 °C; Dodson, 1973), therefore, can be interpreted as the minimum age of the D_2 deformation event within the XFSTB. This is supported by the fact that undeformed post-tectonic granites within the SCB have U–Pb zircon ages of 172–182 Ma (Wang et al., 2003a).

The onset timing of the D_2 deformation event cannot be precisely constrained for the XFSTB. However, the syntectonic peraluminous granites east of the JXSH, which are considered the products of anatexis in the crustal thickening setting (Wang et al., 2002), yielded the U–Pb zircon ages of 220–244 Ma (HBGMR, 1988; Wang et al., in press). The peraluminous granites in other areas within the SCB similar to the Xuefengshan syntectonic granites have SHRIMP zircon U–Pb ages of 230–239 Ma (Xu et al., 2003; Deng et al., 2004). These data suggest that the onset timing of the D_2 deformation event in the XFSTB is likely during the middle Triassic (~244 Ma). This is also supported by the geological observations in the study area: (1) the upper Triassic–lower Jurassic sequences have similar structural styles to those of the pre-Triassic strata (Chen, 1999); (2) the upper Triassic–lower Jurassic rocks unconformably overlie the Devonian–lower Triassic sequences and unconformably underlie the undeformed middle Jurassic–Cretaceous terrestrial clastics (Yan et al., 2003).

5. Discussion and conclusions

5.1. Tectonic model of the Indosinian XFSTB

Several structural features can be summarized for the XFSTB based on the above descriptions: (1) D_2 deformation event occurred between the middle Triassic and early Jurassic (244–195 Ma); (2) most shear zones, faults, cleavages, and axial planes of folds are parallel or subparallel to each other, probably indicating that they are the products of the same deformation event (D_2); (3) some shear zones and faults probably coalesce at depth (see Fig. 2c); (4) the SE- and ESE-dipping shear zones and faults most likely represent major thrusts, while the NW- and WNW-dipping shear zones and faults represent back thrusts; (5) these opposite-dipping shear zones and faults probably form an asymmetric positive flower structure; and (6) the ductile shear zones also have a subsidiary sinistral strike-slip component.

Synthesis of all the structural observations points to a nearly NW–SE shortening stress field for the Indosinian kinematic system in the XFSTB. This system is characterized by the top-to-NW thrusting (dominant) and top-to-SE back-thrusting, accompanied by a sinistral strike-slip movement along the NE- and NNE-trending shear zones and faults. The XFSTB is most likely an Indosinian convergence-dominated transpressive zone rather than a simple, symmetrical convergent zone. Therefore, we propose an oblique convergent or transpressive model, in combination with tectonic wedging and back-thrusting above a low-angle, SE-dipping basal detachment fault. This is analogous to the model proposed for the Teslin tectonic zone (Stevens and Erdmer, 1996).

Fig. 8a conceptually summarizes the major structural features along a NW–SE cross-section through the XFSTB, and Fig. 8b presents a carton illustration of the oblique convergent or transpressive model. An important component of the model is the development of a deep-seated, low angle detachment fault beneath the XFSTB. Based on the greenschist metamorphic conditions in the studied area, the basal detachment fault and transpressive deformation probably occurred at middle crustal levels. All the structural elements are the result of roughly NW-directed transpressive transport along the middle crustal basal detachment (Fig. 8b). The presence of the basal detachment is supported by (1) the geophysical data of the South China Geosciences Transect imaged a low-angle, SE-dipping low-velocity zone (interpreted as a detachment shear zone) at a depth of 12–20 km within the XFSTB (Yuan et al., 1989; Qin, 1991); and (2) the coalescence of shear zones and faults at depth and the dominance of top-to-NW thrusting. During early convergence, the Xuefengshan slices as part of the middle/upper crust of the Yangtze block moved obliquely northwestward along the detachment above the more rigid Yangtze middle/lower crust tectonic wedge (see Fig. 8b). Continuous oblique convergence resulted in significant crustal thickening and upward extrusion. This in turn led to the development of a positive flower structure consisting of opposite-dipping thrusts with a sinistral strike-slip component (also see Richard and Krantz, 1991; Ellis et al., 1998), similar to those of the Pyrenees Orogen (Vergés et al., 1992) and the Klagenfurt Basin in the Eastern Alps (Nemes et al., 1997; Neubauer et al., 2000), and also to the deformation style demonstrated by the sandbox experiments for the development of thrust wedges (Gutscher et al., 1998; Cobbold et al., 2001).

5.2. Implications for the Indosinian tectonics of the SCB

As mentioned in the Introduction, Hsü et al. (1988, 1990), Chen (1999) and Yan et al. (2003) proposed that the Mesozoic tectonics of the SCB was dominated by thrusting, while other authors presented evidences for regional

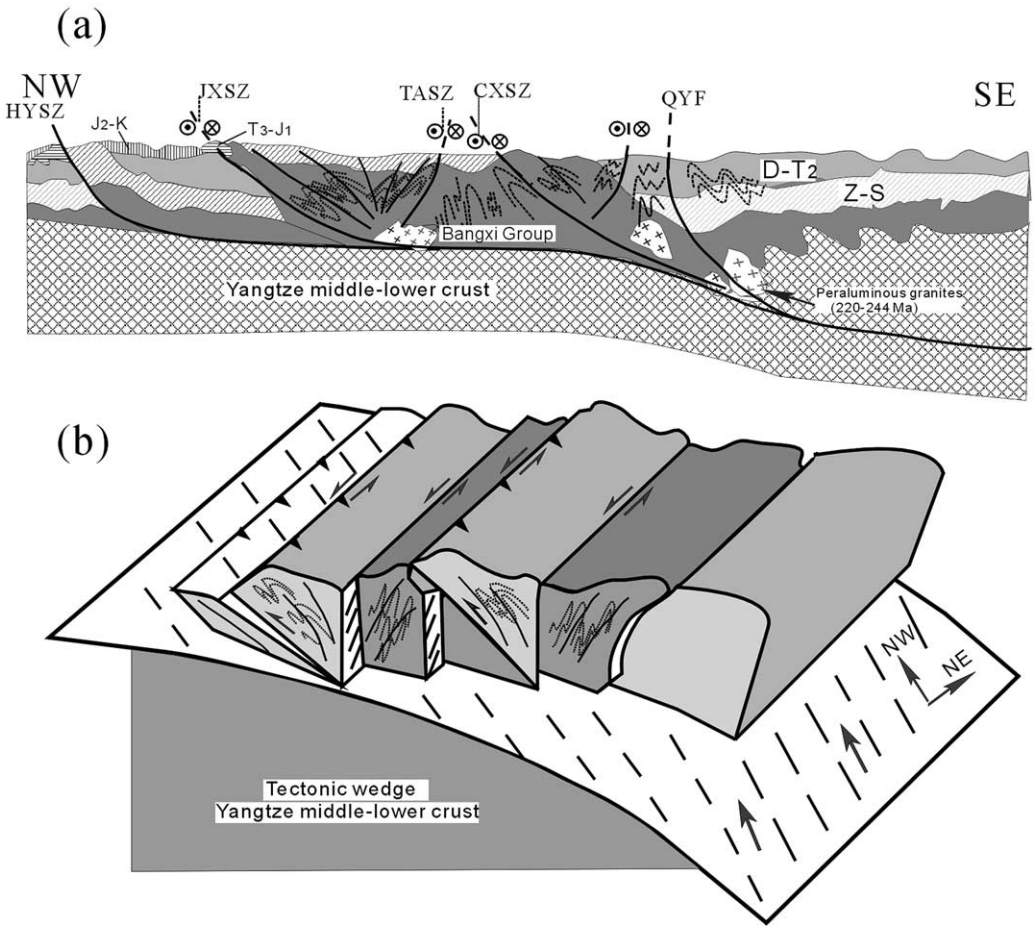

Fig. 8. (a) A synthetic NW–SE section across the XFSTB. (b) Carton illustrating the model of oblique convergence/transpression with tectonic wedging above a low-angle basal detachment. The partitioning of NW-directed thrusting, SE-directed back thrusting, and subsidiary sinistral strike-slip along the NE-trending faults resulted in the structural array of the XFSTB. See text for more information.

extension (Charvet et al., 1994; Faure et al., 1996; Lin et al., 2000; Ren et al., 2002). Xu et al. (1993) and Li et al. (2001) advocated the significance of strike-slip faulting in the SCB. The weakness of these proposals is highlighted by the lack of support from systematic structural and geochronological data. Our new data have provided an important constraint on the timing and kinematics of deformation in the region, that is, the XFSTB is an Indosinian oblique convergent zone dominated by top-to-NW thrusting with a subsidiary sinistral strike-slip component. The XFSTB is representative of the structural style of the SCB west of the Chenzhou–Linwu fault (see Fig. 1a for location). Chen (1999) reported that deformation east of the Chenzhou–Linwu fault intensifies from NW to SE and major thrust faults and folds verge toward the SE. The deformation styles on the two sides of the Chenzhou–Linwu fault seem to form a huge Indosinian positive flower-like structure within the SCB.

Paleomagnetic and paleogeographical data in the SCB suggested that the west-directed subduction of the Pacific Plate occurred later than 125 Ma (Engebretson et al., 1985). There is insufficient evidence to support the existence of Indosinian oceanic basins and contemporaneous ophiolite suites and island-arc magmatism within the SCB (Gupta, 1989; Rowley et al., 1989). In contrast, more and more data support the development of a Neoproterozoic–early Paleozoic rift between the Yangtze and Cathaysian blocks with a sedimentary thickness of greater than 10 km (Goodel et al., 1991; Wang and Li, 2003). The rift represents a weak zone sandwiched between the surrounding stronger Yangtze and Cathaysian blocks. Numerical modeling of continental collision involving a weak zone showed that continental deformation was primarily absorbed by the weak zone when the bounding continental blocks acted as the strong vise (Willett et al., 1993; Willett and Pope, 1996; Ellis et al., 1998). Analogue experiments also demonstrated that the case with a weak zone exhibits thrusting and strike-slip faulting in a diffuse manner (Schreurs, 1994). Consequently, we consider that the huge structural fan within the SCB is a product of the Indosinian intracontinental collision involving a rift weak zone, similar to the type-3 vise model proposed by Ellis et al. (1998). The XFSTB is a part of the weak zone, equivalent to the western flank of the huge structural fan within the SCB, and represents the surface exposed boundary between the Yangtze and Cathaysian

blocks. Therefore, the XFSTB can be interpreted mainly as an Indosinian thrust sheet with some strike-slip shearing component rather than a Triassic ophiolite mélange, as previously thought by Hsü et al. (1988, 1990).

Acknowledgements

The authors would like to thank She Fa Chen, Cees Passchier and an anonymous reviewer for critical and constructive comments and suggestions. We thank X.-H. Li for helpful discussions and suggestions. X.-Q. Liang and C.-L. Liao are thanked for their help during fieldwork. This study was jointly supported by grants from the Natural Science Foundation of China (40334039, 49973021 and 40421303).

References

Bouchez, J.L., Lister, G.S., Nicolas, A., 1983. Fabric asymmetry and shear sense in movement zones. Geologische Rundschau 72, 401–420.

Braun, J., Beaumont, C., 1995. Three dimensional numerical experiments of strain partitioning at oblique plate boundaries: implications for contrasting tectonic styles in the southern Coast Ranges, California and central South Island, New Zealand. Journal of Geophysical Research 100, 10859–18074.

Charvet, J., Lapierre, H., Yu, Y.W., 1994. Geodynamics significance of the Mesozoic volcanism of southeastern China. Journal of Southeast Asian Sciences 9 (4), 387–396.

Chen, A., 1999. Mirror thrusting in the south China Orogenic belt: tectonic evidence from western Fujian, southeastern China. Tectonophysics 305, 497–519.

Cobbold, P., Gapais, D., Means, W.D., Treagus, S.H., 1987. Shear criteria in rocks. Journal of Structural Geology 9, 1–778.

Cobbold, P.R., Durand, S., Mourgues, R., 2001. Sandbox modeling of thrust wedges with fluid-assisted detachments. Tectonophysics 334, 245–258.

Dalrymple, G.B., Lanphere, M.A., 1971. $^{40}Ar/^{39}Ar$ technique of K/Ar dating: a comparison with the conventional technique. Earth and Planetary Science Letters 12, 300–308.

Deng, X.G., Chen, Z.G., Li, X.H., 2004. SHRIMP U–Pb zircon dating of the Darongshan–Shiwandashan. Geological Review 50 (4), 426–432.

Dodson, M.H., 1973. Closure temperature in cooling geochronological and petrological systems. Contributions to Mineralogy Petrology 40, 259–274.

Ellis, S., Beaumont, B., Jamieson, R.A., Quinlan, G., 1998. Continental collision including a weak zone: the vise model and its application to the Newfoundland Appalachians. Canadian Journal of Earth Sciences 35, 1323–1346.

Engebretson, D.C., Cox, A., Gordon, R.G., 1985. Relative motions between oceanic and continental plates in the Pacific basins. Geological Society of America Special Paper 206, 1–59.

Faure, M., Sun, Y., Shu, L., Monié, P., Charvet, J., 1996. Extensional tectonics within a subduction-type orogen: the case study of the Wugongshan dome (Jiangxi Province, southeastern China). Tectonophysics 263, 77–106.

Gilder, S.A., Gill, J., Coe, R.S., Zhao, X.X., Liu, Z.W., Wang, G.X., 1996. Isotopic and paleomagnetic constraints on the Mesozoic tectonic evolution of South China. Journal of Geophysical Research 107 (B7), 16137–16154.

Goodel, P.C., Gilder, S., Fang, X., 1991. A preliminary description of the Gan-Hang failed rift, southeastern China. Tectonophysics 197, 245–255.

Gupta, S., 1989. Comment and reply on "Mesozoic overthrust tectonics in South China". Geology 17, 669–671.

Gutscher, M.A., Kukowski, N., Malavieille, J., Lallemand, S., 1998. Episodic imbricate thrusting and underthrusting: analog experiments and mechanical analysis applied to the Alaskan Accretionary Wedge. Journal of Geophysical Research 103, 10161–10176.

Harrison, T.M., Duncan, I., McDougall, L., 1985. Diffusion of ^{40}Ar in biotite: temperature, pressure and compositional effects. Geochimica et Cosmochimica Acta 49, 2261–2468.

HBGMR (Hunan Bureau of Geology and Mineral Resources), 1988. Regional Geology of the Hunan Province.. Geological Press, Beijing, pp. 286–507 (in Chinese with English summary).

Hiroshi, Y., 1994. Kinematics of mylonitic rocks along the Median Tectonic Line, Akaishi Range, central Japan. Journal of Structural Geology 16 (1), 61–70.

Holloway, N.H., 1982. North Palawan Block, Philippines: its relation to Asian mainland and role in evolution of South China Sea. American Association of Petroleum Geologists Bulletin 66, 1355–1383.

Hsü, K.J., Sun, S., Li, J.L., Chen, H.H., Sengör, A.M.X., 1988. Mesozoic overthrust tectonics in South China. Geology 16, 418–421.

Hsü, K.J., Li, J.L., Chen, H.H., Wang, Q.C., Sun, S., Sengör, A.M.X., 1990. Tectonics of South China: key to tectonics of South China: key to understanding west Pacific geology. Tectonophysics 193, 9–39.

Jia, B.H., 1992. The ductile shear tectonic zones in Xuefengshan region. Hunan Geology 11 (3), 203–208 (in Chinese with English abstract).

Jia, B.H., 1994. Structural signatures of Xuefengshan area, Hunan Province. Regional Geology of China 1, 65–71 (in Chinese with English abstract).

Law, R.O., 1990. Crystallographic fabrics: a selective review of their applications to research in structural geology. In: Knipe, R.J., Rutter, E.H. (Eds.), Deformation Mechanism, Rheology and Tectonics Geological Society Special Publication, vol. 54, pp. 335–352.

Li, J.W., Zhou, M.F., Li, X.F., Fu, Z.R., Li, Z.J., 2001. The Hunan–Jiangxi strike-slip fault system in southern China: southern termination of the Tanlu fault. Journal of Geodynamics 32, 333–354.

Li, X.H., McCulloch, M.T., 1996. Secular variation in the Nd isotopic composition of Neoproterozoic sediments from the southern margin of the Yangtze block: evidence for a Proterozoic continental collision in southeast China. Precambrian Research 76, 67–76.

Li, X.H., Chung, S.L., Zhou, H.W., Lo, C.H., Liu, Y., Chen, C.H., 2004. Jurassic intraplate magmatism in southern Hunan–eastern Guangxi: $^{40}Ar/^{39}Ar$ dating, geochemistry, Sr–Nd isotopes and implications for tectonic evolution of SE China. In: Malpas, J., Fletcher, C.J., Aitchison, J.C., Ali, J. (Eds.), Aspects of the Tectonic Evolution of China Geological Society, London, Special Publications, vol. 226, pp. 193–216.

Li, Z.X., 1998. Tectonic history of the major East Asian lithospheric blocks since the mid-Proterozoic: a synthesis. In: Flower, M.F.J., Chung, S.L., Lo, C.H., Lee, C.Y. (Eds.), Mantle Dynamics and Plate Interactions in East Asia American Geophysical Union (Geodynamic Series), vol. 27, pp. 221–243.

Lin, W., Faure, M., Monié, P., Schärer, U., Zhang, L.S., Sun, Y., 2000. Tectonics of SE China: new insights from the Lushan massif (Jiangxi Province). Tectonics 19 (5), 852–871.

Maluski, H., Rajlich, P., Matte, P., 1993. $^{40}Ar/^{39}Ar$ dating of the Inner Carpathians Variscan basement and Alpine mylonitic overprinting. Tectonophysics 223, 313–337.

Nemes, F., Neubauer, F., Cloetingh, S., Genser, J., 1997. The Klagenfurt Basin in the Eastern Alps: an intra-orogenic decoupled flexural basin? Tectonophysics 282, 189–203.

Neubauer, F., Fritz, F., Genser, J., Kurz, W., Nemes, F., Wallbrecher, W., Wang, X., Willingshofer, E., 2000. Structural evolution within an

extruding block: model and application to the Alpine–Pannonian. In: Lehner, F.K., Urai, J.L. (Eds.), Aspects of Tectonic Faulting. Springer-Verlag, Berlin. pp. 141–153.

Purdy, J.W., Jäger, E., 1976. K–Ar ages on rock-forming minerals from the Central Alps. Mem. 1st Geol. Min. Univ. Padova, 30.

Qin, B.H., 1991. Deep-seated structure beneath Hunan Province revealed by Taiwang–Heishui geotravers. Hunan Geology 15, 89–96 (in Chinese with English abstract).

Ren, J.Y., Tamaki, K., Zhang, J.X., 2002. Late Mesozoic and Cenozoic rifting and its dynamic setting in eastern China and adjacent areas. Tectonophysics 344, 175–205.

Richard, P., Krantz, R.W., 1991. Experiments on fault reactivation in strike-slip mode. Tectonophysics 188, 113–117.

Rowley, D.B., Ziegler, A.M., Nie, G., 1989. Comment on "Mesozoic overthrust tectonics in South China". Geology 17, 384–386.

Sang, H.Q., Wang, S.S., Qiu, J., 1996. The ^{40}Ar–^{39}Ar ages of pyroxene, hornblende and plagioclase in Taipingzhai granulites in Qianxi County, Hebei Province and their geological implications. Acta Petrologica Sinica 12 (4), 390–400 (in Chinese with English abstract).

Schreurs, G., 1994. Experiments on strike-slip faults and block rotation. Geology 22, 567–570.

Simpson, C., Schmid, S., 1983. An evaluation of criteria to deduce the sense of movement in sheared rocks. Geological Society of America Bulletin 94, 1281–1288.

Stevens, R.A., Erdmer, P., 1996. Structural divergence and transpression in the Teslin tectonic zone, southern Yukon Territory. Tectonics 15 (6), 1342–1363.

Tullis, J., Christie, J.M., Griggs, D.T., 1973. Microstructure and preferred orientations of experimentally deformed quartzites. Geological Society of America Bulletin 84, 297–314.

Twiss, R.J., Moores, E.M., 1994. Structural Geology. W.H. Freeman and Company, New York, pp. 215–422.

Vergés, J., Muňoz, J.A., Martínez, A., 1992. South Pyrenean fold and thrust belt: the role of foreland evaporitic levels in thrust geometry. In: McClay, K.R. (Ed.), Thrust Tectonics. Chapman & Hall, London, pp. 255–264.

Wang, J., Li, Z.X., 2003. History of Neoproterozoic rift basins in South China: implications for Rodinia break-up. Precambrian Research 122 (1–4), 141–158.

Wang, J., Li, X.H., Duan, T.Z., Liu, D.Y., Song, B., Li, Z.X., Gao, Y.H., 2003. Zircon SHRIMP U–Pb dating for the Cangshuipu volcanic rocks and its implications for the lower boundary age of the Nanhua strata in South China. Chinese Science Bulletin 48 (16), 1663–1679.

Wang, Y.J., Zhang, Y.H., Fan, W.M., Xi, X.W., Guo, F., Lin, G., 2002. Numerical modeling for generation of Indo-Sinian peraluminous granitoids Hunan Province: basaltic underplating vs tectonic thickening. Science in China (D series) 45 (11), 1042–1056.

Wang, Y.J., Fan, W.M., Guo, F., 2003a. Geochemistry of early Mesozoic potassium-rich dioritic–granodioritic intrusions in Southeastern Hunan Province, South China: petrogenesis and tectonic implications. Geochemical Journal 37 (4), 427–448.

Wang, Y.J., Fan, W.M., Guo, F., Peng, T.P., Li, C.W., 2003b. Geochemistry of Mesozoic mafic rocks around the Chenzhou–Linwu fault in South China: implication for the lithospheric boundary between the Yangtze and the Cathaysia Blocks. International Geology Review 45 (3), 263–286.

Wang, Y.J., Fan, W.M., Peng, T.P., Guo, F., 2005. Element and Sr–Nd systematics of early Mesozoic volcanic sequence in southern Jiang Province, South China: petrogenesis and tectonic implications. International Journal of Earth Sciences 94 (1), 53–65.

Wang, Y.J., Fan, W.M., Liang, X.Q., Peng, T.P., Shi, Y.R. SHRIMP zircon U–Pb geochronology of Indosinian granites in Hunan Province and its petrogenetic implications. Chinese Science Bulletin, in press.

Willett, S., Pope, D., 1996. Thermo-mechanical modeling of orogenic plateau growth by crustal thickening. In: American Geophysical Union, Abstracts, Fall meeting, December 1996. EOS 77(supp), F688.

Willett, S., Beaumont, C., Fullsack, P., 1993. A mechanical model for the tectonics of doubly vergent compressional orogens. Geology 21, 371–374.

Xu, J.W., Ma, G., Tong, W.X., Zhu, G., Lin, S., 1993. Displacement of the Tancheng–Lujiang wrench fault system and its geodynamic setting in the northwestern Circum-Pacific. In: Xu, J. (Ed.), The Tanchang–Lujiang Wrench Fault System. John Wiley & Sons, pp. 51–74.

Xu, X.S., Deng, P., O'Reilly, S.Y., 2003. Single zircon LAM ICPMS U–Pb dating of Guidong complex (SE China) and its petrogenetic significance. Chinese Science Bulletin 48 (17), 1892–1899.

Yan, D.P., Zhou, M.F., Song, H.L., Wang, X.W., Malpas, J., 2003. Origin and tectonic significance of a Mesozoic muti-layer over-thrust system within the Yangtze bock (South China). Tectonophysics 361, 239–254.

Yin, C.Y., Liu, D.Y., Gao, L.Z., Wang, Z.Q., Xing, Y.S., Jian, P., Shi, Y.R., 2003. Lower boundary age of the Nanhua system and the Gucheng glacial stage: evidence from SHRIMP II dating. Chinese Science Bulletin 48 (16), 1657–1662.

Yuan, X.C., Zuo, Y., Cai, X.L., Zhu, J.S., 1989. The structure of the lithosphere and the geophysics in the South China Plate. In: Editorial Board of Bulletin of Geophysics (Eds.), Progress on Geophysics in China in the 1980s, Beijing, pp. 243–249.

Zhou, X.M., Li, W.X., 2000. Origin of Late Mesozoic igneous rocks in Southeastern China: implications for lithosphere subduction and underplating of mafic magmas. Tectonophysics 326, 269–287.